DEM-BASED CALIBRATION OF SOIL CONTACT PARAMETERS PRIOR TO GRAPEVINE BURYING
/
基于离散元法的葡萄藤埋前土壤接触参数标定

Beibei ZHANG[1)], Julaiti MAITIROUZI*[1)], Shixiang XING[1)], Hongcheng DENG[2)], Wenjing BAI[2)], Haileeqguli YASEN[2)]
[1)] College of Mechanical Engineering, Xinjiang University, Urumqi / China;
[2)] Turpan Agricultural and Rural Mechanization Development Center, Turpan / China
Tel: +86 13986888714; E-mail: 13986888714@163.com
DOI: https://doi.org/10.35633/inmateh-76-20

Keywords: *grapevine, discrete element method, static and dynamic angle of repose, soil, parameter calibration, grapevine burying machine.*

ABSTRACT
To address the lack of simulation parameters when applying discrete element simulations to guide the optimal design of grapevine burying machines, this study focused on the soil conditions in Xinjiang. The soil was divided into three layers, and the static and dynamic angle of repose characteristics of each layer were investigated using the Hertz-Mindlin with Johnson-Kendall-Roberts (JKR) contact model. First, the Plackett-Burman test was used to eliminate parameters that had no significant effect on the static and dynamic angles of repose. Then, the steepest ascent test was applied to narrow the parameter ranges, followed by the Box-Behnken test to develop regression models between the repose angles and the significant parameters. The results showed that the soil-soil restitution coefficient, soil-soil rolling friction coefficient, soil-steel static friction coefficient, and JKR surface energy were the key parameters influencing the static and dynamic repose angles. Experimental validation demonstrated that the average relative errors between the simulated and measured angles of repose using the optimized parameters were 0.92% and 0.32%, respectively, confirming the validity of the selected parameters. This study provides an important reference for the design optimization of grapevine burying machines and for discrete element simulation of other cohesive particulate materials.

摘要
针对应用离散元仿真指导葡萄埋藤机优化设计时仿真参数缺乏的问题。以新疆土壤为研究对象，将土壤分为三层，以 "Hertz-Mindlin with Johnson-Kendall-Roberts"为接触模型，研究了不同土层的静/动态休止角特性。首先利用 Plackett-Burman 检验排除对静/动态休止角影响不显著的参数，利用最陡爬坡检验缩小参数区间范围，利用 Box-Behnken 检验得到静/动态休止角与显著性参数之间的回归模型。结果发现，土-土恢复系数、土-土滚动摩擦系数、土-钢静摩擦系数和 JKR 表面能是影响静/动态休止角的主要参数。通过实验验证，最优离散元模拟参数的静/动态休止角与实测值的平均相对误差分别为 0.92% 和 0.32%，验证了所选参数的有效性，该研究为葡萄埋藤机的优化设计以及其他粘性颗粒物料的离散元模拟提供了重要参考。

INTRODUCTION
In Northwest China, much of the agricultural land in arid irrigated regions is used to cultivate grapes as a specialty crop. In 2021, Xinjiang alone accounted for 1.85 million acres of grape cultivation, producing 3.5 million tons, ranking first in both production and planting area nationwide *(Wang et al., 2024)*. Grapevine burying is a key winter protection technique for grapes in northern China, with its production costs comprising nearly 50% of the annual expenses. Turpan, as the largest grape-growing base in Xinjiang, has seen a rapid increase in mechanized vine-burying, and while the current mechanization level is relatively high, there remain significant shortcomings in terms of efficiency, cost, and adaptability. A major challenge lies in the lack of advanced machinery to further improve productivity (*Shen et al., 2024*). Therefore, the design of suitable agricultural machinery is crucial. In this context, soil modeling plays a vital role in the development and optimization of such equipment, as it contributes to increased production efficiency and reduced operational costs. However, no discrete element simulation models currently exist for soil prior to grapevine mulching and burial. Thus, it is essential to construct a discrete element parameter model of the soil.

To analyse the interaction between soil-engaging components and soil, numerical simulation is commonly used to establish an accurate soil model (*Smith et al., 2014*).

BeiBei Zhang, M.S.Stud. Eng.; Julaiti Maitirouzi, Prof. Ph.D. Eng.; Shixiang Xing, M.S. Stud. Eng.; Honcheng Deng, Senior engineer. M.S. Eng.; Wenjing Bai, Senior engineer. M.S. Eng.; Haileeqguli Yasen, Senior engineer. M.S. Eng.

Xinjiang region is an irrigated area with high evaporation in the surface layer, and there is a large difference in water content between the surface soil and the subsoil, which has a large impact on the contact parameters of the discrete element model (*Li et al., 2019*).

Some scholars have conducted layered sampling of cold-proof soil during grapevine clearing to determine the moisture content of different soil layers. Based on this data, they combined it with simulation tests of the soil's angle of repose to complete discrete element parameter calibration, achieving results with minimal error *(Yang et al., 2023)*. Some scholars have constructed a particle model of mulberry soil under specific moisture conditions based on the soil particle size distribution. Using this model, the discrete element parameters of the soil were calibrated, and the results were found to be reliable (*Song et al., 2022*). The combination of static and dynamic angles of repose for calibrating discrete element particles has been widely applied in fields such as food, pharmaceuticals, industrial materials, and agricultural soils, yielding promising results. The calibrated soil simulation results closely match experimental measurements and meet the intended testing objectives (*Zhang et al., 2024; Luana et al., 2017; Li S. et al., 2024*). In addition, some researchers have applied scaling theory to calibrate the contact parameters in discrete element simulations of wheat flour, using the Plackett-Burman test, steepest ascent test, and Box-Behnken design, with the static angle of repose as the response variable (*Li et al., 2019*).

Most existing soil discrete element simulation parameter calibrations rely on a single static angle of repose as the response variable, without incorporating a combination of static and dynamic angles of repose to evaluate soils with varying moisture content. However, in real-world operations, soil exhibits both static and dynamic behaviours, and using both angles of repose as response variables offers a more accurate representation of the soil's actual mechanical state during field operations (*Zeng et al., 2019*). In Xinjiang, field soil conditions are typically assessed prior to grapevine burying, and in some areas, pre-irrigation is performed to ensure sufficient soil moisture. This results in more cohesive soil, which helps improve the performance and effectiveness of the grapevine burying operation (*Maitadudulili.et al., 2016*).

In this study, the Hertz-Mindlin with Johnson-Kendall-Roberts (JKR) contact model was selected to calibrate the contact parameters of the soil DEM model for different soil layers. The Plackett-Burman (PB) experimental design was first used to screen for significant factors and to analyse their effects on the static and dynamic angles of repose. Subsequently, a Box-Behnken experimental design with multi-objective optimization was applied to determine the candidate discrete element parameter sets for each soil layer. Finally, the calibrated discrete element simulation parameters were experimentally validated. The resulting optimal DEM parameters provide accurate input data for the simulation of grapevine burying operations, and also serve as a reference for discrete element modeling of other cohesive particulate materials.

MATERIALS AND METHODS

Materials and Instruments

The samples of vineyard soil were taken from the planting base of Thompson Seedless in Lianmuqin Township, Shanshan County, Turpan City, Xinjiang Uygur Autonomous Region (42.87°N,89.98°E). Based on the depth of soil disturbance during vineyard operation, the 60 cm soil profile affected by machinery was divided into three layers: the upper layer (0-20 cm), the middle layer (20-40 cm), and the lower layer (40-60 cm). Tests on the soil characterization parameters were conducted in accordance with the Chinese standard GB/T 50123–1999, Standard for Geotechnical Test Methods.

Test apparatus included the following equipment: an FCE-3000 electric constant temperature blast drying oven; a standard ring knife (specifications: diameter 50.46 mm, height 50 mm); a JJ623BF electronic balance (range: 620 g, precision: 1 mg); a standard test sieve set conforming to GB/T 6003–1997, with mesh sizes from top to bottom of 2.0 mm, 1.0 mm, 0.5 mm, 0.25 mm, and 0.075 mm; customized cylinder 1 (inner diameter 40 mm, height 100 mm); customized cylinder 2 (inner diameter 100 mm, height 100 mm); 65Mn iron sheet; 42 stepper motor; flange coupling; metal support; aluminium alloy profiles; a 200-type standard inspection sieve machine; aluminium box; camera; and food preservation bags, among other auxiliary tools.

Intrinsic parameter measurements

The ring knife method was used to measure soil density. In the field, the soil surface was paved and compacted, and the soil was taken with a ring knife, which was placed in an aluminium box and a food preservation bag to preserve the soil sample. After picking out the plant stalks and other impurities in the soil, the total mass of the ring cutter and soil was determined using an electronic balance and recorded as m1, and the mass of the empty ring cutter was determined as m0. Five-point sampling method was used to sample the

soil in three layers, and the average density of soil in the three layers from the top to the bottom was 172.23 kg/m^3, 177.35 kg/m^3, and 177.69 kg/m^3, and the average density of the soil was taken to be 175.76 kg/m^3.

$$\rho = \frac{m1-m0}{v} \quad (1)$$

where: ρ is the soil density (g·cm^{-3}); v is the volume of the ring knife (cm^3); m_1 is the mass of the ring knife and soil *(g);* and m_0 is the mass of the ring knife (g).

The drying method was used to determine soil moisture content. First, the mass m' of the empty aluminium box was measured using an electronic balance. Then, soil was added, and the total mass m' of the box and moist soil was recorded. The box was placed in a preheated oven at (107±2)℃ for 8 hours, cooled to room temperature, and weighed again to obtain the mass after drying.

$$\omega = \frac{m_1 - m_2}{m_1 - m} \quad (2)$$

where:

ω is the moisture content of the soil (%);

m_1 is the mass of the aluminium box and the soil (g);

m_2 is the mass of the aluminium box and the dry soil (g);

m is the mass of the aluminium box (g).

Sieving method was used to measure the particle size distribution of the soil. Soil collected from the field was first dried in a drying oven to remove impurities and pulverized, and then sieved using standard test sieves and oscillating sieves to measure the mass of the soil at different particle sizes and calculate the percentages as shown in Table 1.

Table 1

Soil particle size distribution

Particle radius/mm	Mass/g	Percent/%
≥2	17.48	8.74
2-1	8.34	4.17
1-0.5	11.68	5.84
0.5-0.25	41.50	20.75
0.25-0.075	111.60	55.80
0.075-0	9.40	4.70

According to the soil texture classification standard GB/T 17296, soil with a sand content greater than 50% is classified as clayey soil. Based on this standard, the soil in the study area was identified as clayey sandy loam (*Chen et al., 2017*).

Using the drying method and the addition of pure water, three soil moisture content gradients - 8.39%, 10.74%, and 12.40% - were prepared for the angle of repose tests. A dried soil sample with mass m_3 was measured, and pure water with mass m_1 was added. The mixture was stirred thoroughly and allowed to stand for 24 hours. The actual moisture content ω_x was then determined using the drying method and calculated as follows:

$$\omega_x = \frac{m_s}{m_s+m_3} \quad (3)$$

where*:*

ω_x is the water content of the soil (%);

m_s is the mass of water required to configure the sample (g);

m_3 is the sample mass (g).

Static angle of repose measurement

Common methods for measuring the static angle of repose include the cylinder lifting method and the funnel method (*Han et al., 2020; Zhen et al., 2020*). Given that the soil in this study contains some moisture and exhibits relatively cohesive texture, the hollow cylinder method was considered more suitable for accurately determining the static angle of repose. The test was conducted by placing a 65Mn steel plate horizontally on the test machine platform. The cylinder test apparatus was then connected, and the cylinder was positioned vertically on the steel plate and filled with the test soil.

The test machine was activated to lift the cylinder at a uniform speed of 25 mm/s (*Thomas et al., 2018*). A camera was used to record the formation of the soil pile for each moisture content condition. The test was repeated four times for each condition to ensure repeatability. The actual test setup for measuring the static angle of repose is shown in Fig. 1.

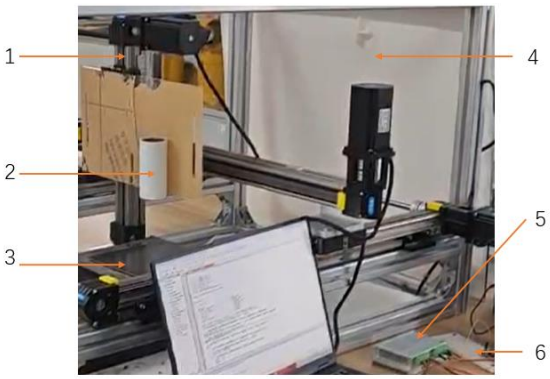

Fig. 1 - Static angle of repose measurement

1. Slipway; 2. Cylinder; 3. Cushion; 4. Background Board; 5. Driver; 6. Controller.

Image processing was used to determine the soil accumulation angle values (*Luo et al., 2018*). First, the original image was cropped to an appropriate size, and then processed through grayscale conversion and binarization. The boundary coordinates of the soil pile were extracted using the image digitizing function in Origin software (Fig. 2d). For each set of coordinates, linear fitting was performed, and the corresponding scatter plots and fitted lines were generated to obtain the fitting equations. The slope of each fitted line was then used to calculate the accumulation (stacking) angle. The arctangent (inverse tangent) of the slope was converted into an angle value (Fig. 2e). The final stacking angle was obtained by averaging the angles from both sides of each image. The image processing procedure and results are illustrated in Fig. 2.

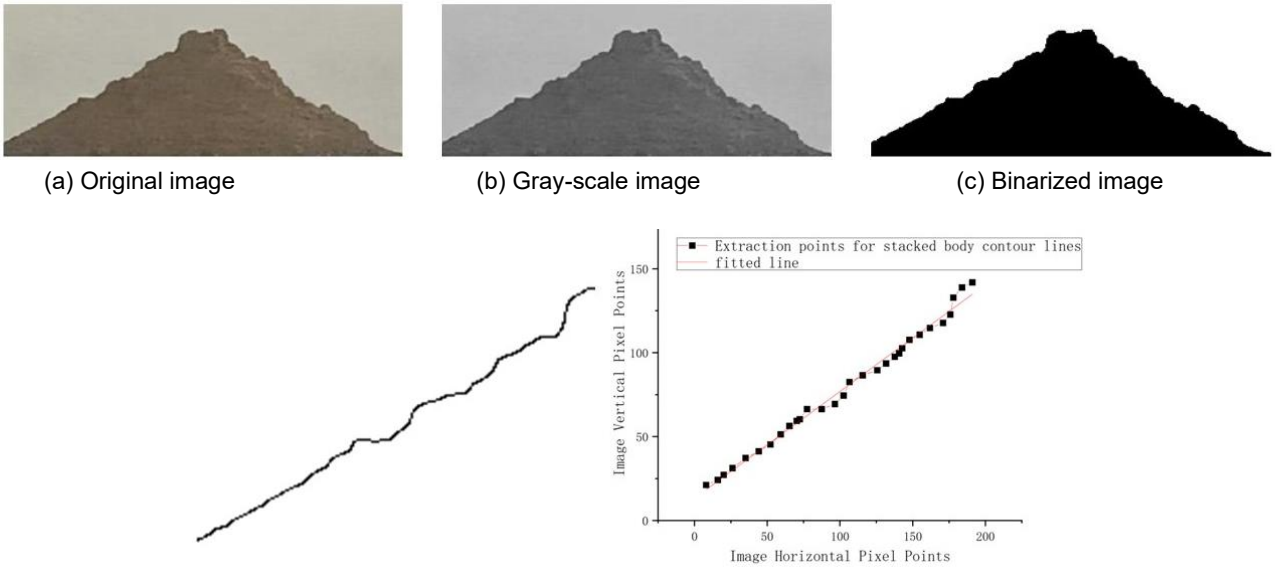

(a) Original image (b) Gray-scale image (c) Binarized image

(d) Contour Extraction Line Image (e) Fitted line

Fig. 2 - Calculation process of static angle of repose of soil

Dynamic angle of repose measurement

The dynamic angle of repose is defined as the maximum angle between the slope of the soil mass and the horizontal plane before collapse occurs, i.e., when the internal forces between soil particles can no longer counteract gravity as the soil ascends with the rotation of the drum. It serves as a key parameter for characterizing the dynamic flow behaviour of soil. A custom-built device was used to measure the dynamic angle of repose, as illustrated in Figure 3.

The apparatus consists of a rotating drum (100 mm in diameter and 100 mm in length, with a steel sheet affixed to the inner wall), a motor, controller, and coupling. The measurement procedure was as follows: a specified amount of soil was loaded into the drum until the fill level reached 25% of the drum volume.

The motor was then activated to rotate the drum at a constant speed of 7 r/min, as recommended in relevant literature (*Zhou et al., 2023*). A video camera positioned directly in front of the drum recorded the rotation process in real time to capture the dynamic angle of repose. After repeating the experiment for five times, the average values of the dynamic angle of repose α of the three layers of soil were obtained as 42.7°, 43.91° and 45.7°, respectively.

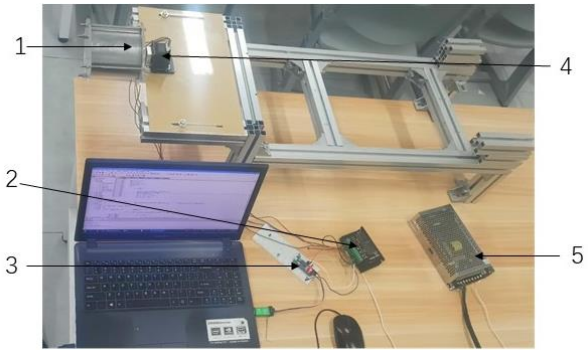

Fig. 3 - Dynamic angle of repose measurement

1. Roller; 2. Driver; 3. Controller; 4. Electric Machine; 5. Power Supply.

Contact model

The water content of the soil before burying the vine is not low, and the soil particles will have a certain degree of adhesion between them. The Hertz-Mindlin with JKR model is used as a particle contact model, which is suitable for simulating the particulate materials that are prone to adhesion and agglomeration effects. Therefore, discrete element simulation was carried out using the Hertz-Mindlin contact model with JKR cohesion model, which assumes that the adhesion force acts within the contact area of the particles and contributes to the contact surface manifolds, thus obtaining a larger contact area than predicted by the Hertz-Mindlin theory. In the JKR model, the normal elastic contact force F_{JKR} of the particles is expressed as:

$$F_{JKR} = \frac{4E^*}{3R^*}\alpha^3 - 4\sqrt{\pi\gamma E^*\alpha^3} \tag{3}$$

$$\delta = \frac{\alpha^2}{R^*}\left[1 - \sqrt{\frac{4\pi\gamma R^3}{E^*\alpha^3}}\right] \tag{4}$$

where: E^* is the equivalent elastic modulus; R^* is the equivalent particle radius; α is the normal overlap; γ is the particle surface energy; δ is the tangential overlap.

The first term in Eq. (3) is the normal contact force based on the Hertz-Mindlin theory, and the second term is the particle adhesion force based on the JKR theory; when the particle surface energy $\gamma = 0$, the JKR model will degenerate into the Hertz-Mindlin model.

Principle of particle stiffness reduction

The Rayleigh time step refers to the length of time for 2 collision operations between particles, which is an important factor affecting the computational efficiency of DEM simulation. The formula for the Rayleigh time step is:

$$t_R = \frac{\pi r}{(0.163\upsilon + 0.877)}\sqrt{\frac{\rho}{G}} \tag{5}$$

where: t_R is the Rayleigh time step; r is the particle radius; υ is the particle Poisson's ratio; ρ is the particle density; G is the particle shear modulus.

To ensure the efficiency and accuracy of the simulation, 10% to 30% of the Rayleigh time step is usually chosen as the computational time step. From Eq. (5), it can be seen that the shear modulus of the particles is the main factor affecting the time step, and the reduction of particle stiffness allows the use of a larger time step in the simulation, which reduces the number of computational iterations and thus improves the computational speed. With the introduction of reduced stiffness particles in the JKR model, more overlap of particles occurs during kinematic collisions. If the surface energy of the particles remains constant, the kinetic energy lost in the collision will increase. In order to ensure that the result of the motion of the particles after the collision remains unchanged, so that the separation energy required by the 2 particles in contact remains constant, the reduction of particle stiffness must be balanced by the reduction of the surface energy of the particles, and the conditions to be satisfied are:

$$\gamma_{mod} = \gamma \left(\frac{G_{mod}}{G}\right)^{2/5} \quad (6)$$

where: γ_{mod} and G_{mod} are the surface energy and shear modulus of the modified particles respectively.

With the reduction of particle stiffness and the increase of time step, the calculation speed is improved, but the range of particle stiffness reduction should be limited. In order to prevent the particle stiffness from decreasing too much and causing too much overlap, the particle shear modulus after decreasing the stiffness should be kept above 10^7 Pa (*Lommen et al., 2023*).

Discrete element simulation parameter calibration

According to the theory of particle scaling, the related literature proposes that if the density of the particles corresponding to the scaled model is kept constant, the intrinsic parameters of the particles corresponding to the scaled model are the same as those of the original model, but the contact parameters of the particles with the particles and the particles with the touching soil parts corresponding to the scaled model can't be obtained directly according to the equations, and the related parameters need to be calibrated by simulation tests (*Feng et al., 2009*).

In order to reduce the amount of simulation data and improve the simulation efficiency, the soil particles are simplified into a single sphere model, and then the scaling theory is used to scale the particles of different particle size ranges into appropriate sizes, referring to the relevant literature (*Zhen et al., 2024; Yang et al., 2023; Li et al., 2024*) and the GEMM database, to determine the range of values of intrinsic parameters of the soil and the relevant contact parameters are shown in the following table.

Table 2

Scaling model parameter value range

Parameters	Value	Unit
Soil density	175.7567	**kg·m^{-3}**
Poisson's ratio for soil	0.33	
Soil shear modulus A	10-10 0	**MPa**
Coefficient of restitution between soil particles B	0.15-0.75	
Coefficient of static friction between soil particles C	0.2-1.16	
Coefficient of rolling friction between soil particles D	0.05-0.15	
Steel density	7850	**kg·m^{-3}**
Steel Poisson's ratio	0.3	
Steel shear modulus	7.9×10^4	**MPa**
Coefficient of restitution between soil-steel E	0.25-0.65	
Coefficient of static friction between soil-steel F	0.30-0.80	
Coefficient of rolling friction between soil and steel G	0.20-0.40	
Surface energy (JKR) H	0.1-0.3	**J·m^{-2}**

Discrete element simulation modeling

In SOLIDWORKS software, the 3D geometric model of the static and dynamic angle of repose measurement device was built according to the scale of 1:1 with reference to the dimensions of the measurement device, saved in STL format and imported into EDEM software. The 3D geometric model of the measurement device is shown in Fig. 4.

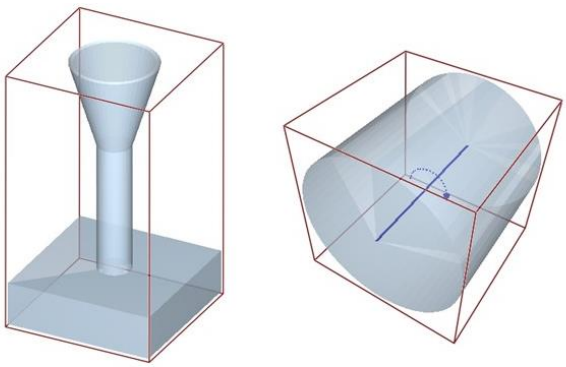

(a) Static angle of repose model (b) Dynamic angle of repose model

Fig. 4 - Geometric model of the static and dynamic angle of repose determination device

The initial conditions of the simulation were set as follows: the particle sizes of the enlarged spherical particles were set to 2.5 mm, 5 mm and 10 mm, and the generation mode was dynamic. The static angle of repose model establishes a particle factory at the top of the funnel, with a total particle mass of 0.167 kg, and the generation rate is set to 0.5 kg of particles per second. In the dynamic angle of repose simulation model, a particle factory was established inside the cylinder to simulate the soil particles. A total particle mass of 0.209 kg was used, corresponding to a 25% fill rate of the drum volume, consistent with the experimental setup. After the particles settled into a stationary state, a rotational axis was introduced at the centre of the model, and the rotational speed was set to 7 r/min. The computational time step for both the dynamic and static repose angle models was set to 2.5 ms. After the particles stabilized, a rotational axis was added to the centre of the model, and the rotational speed was set to 7 r/min. The computational time step for both models was defined as 20% of the Rayleigh time step, and the mesh size was set to three times the diameter of the smallest spherical particle. Once the simulation reached a stable state, the angle of repose was measured using the EDEMPY measurement tool. The discrete element simulation parameters included the intrinsic properties of the particles, the 3D geometric model, the contact parameters between particles, and the contact parameters between particles and the geometry. The 3D geometry was modeled using 65Mn material, and the range of contact parameter variation was determined through preliminary experiments.

Simulated static/dynamic angle of repose determination

To accurately determine the angle of repose of the simulated particle pile, the simulation result files were analysed using the EDEMPY library, a Python-based post-processing tool for discrete element simulations. Measurement principle: First, a radial array of cylindrical containers is defined. The highest particle in each container is then identified. The centre-of-mass coordinates of these particles are extracted and subjected to least-squares linear fitting. The angle between the resulting fitted line and the horizontal plane is calculated, representing the angle of repose. This measurement principle is illustrated in Fig. 5 and Fig. 6. To improve measurement accuracy, only the stable region of the pile was selected for analysis. In addition, measurements were performed along multiple radial directions (eight directions in this study), and the average angle of repose was calculated. A schematic of the multi-directional measurement method is shown in Fig. 7.

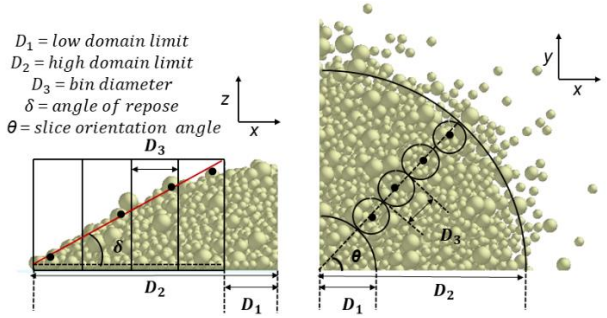

Fig. 5 - Schematic diagram of static angle of repose measurement

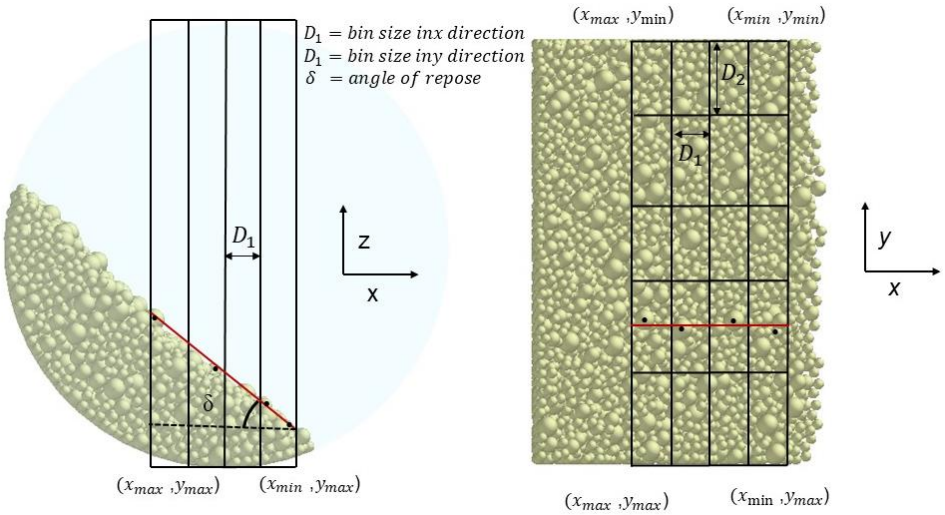

Fig. 6 - Schematic diagram of dynamic angle of repose measurement

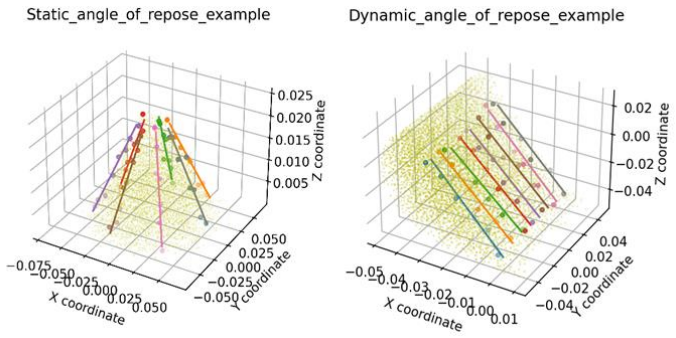

Fig. 7 - Schematic diagram of multiple measurements of angle of repose

RESULTS

Plackett-Burman test for discrete element simulation parameters

Not all parameters set for the discrete element simulation have a significant effect on the angle of repose. To identify the key influencing factors, a parameter screening test was conducted using the Plackett-Burman design in Design-Expert software. The static and dynamic angles of repose were used as response variables, while the eight parameters to be calibrated, along with two dummy variables (as shown in Table 3), were selected as the test factors. This design allowed for the evaluation of each factor's significance on the angle of repose and facilitated the identification of the most impactful parameters for further optimization.

Table 3

Plackett-Burman test scheme and results

Serial number	Experimental factors								Static angle of repose / (°)	Dynamic angle of repose / (°)
	A	B	C	D	E	F	G	H		
1	-1	-1	1	-1	1	1	-1	1	33.33	55.35
2	1	-1	1	1	1	-1	-1	-1	39.44	47.88
3	1	1	1	-1	-1	-1	1	-1	23.57	40.61
4	1	-1	1	1	-1	1	1	1	*45.01*	*61.13*
5	1	-1	-1	-1	1	-1	1	1	31.38	51.45
6	1	1	-1	-1	-1	1	-1	1	27.82	63.35
7	-1	-1	-1	-1	-1	-1	-1	-1	26.82	46.56
8	-1	-1	-1	1	-1	1	1	-1	46.79	50.82
9	-1	1	-1	1	1	-1	1	1	39.27	51.39
10	-1	1	1	1	1	-1	-1	1	32.28	51.25
11	-1	1	1	-1	-1	1	1	-1	27	47.04
12	1	1	-1	1	1	1	-1	-1	36.35	57.19

The test results in Table 3 were analysed by ANOVA, and the significance of each test parameter on the static angle of repose and dynamic angle of repose was obtained as shown in Tables 4 and 5. From Table 4, it can be seen that the rolling friction coefficient of soil-soil D has a $p < 0.01$, which is very significant on the simulation results; soil-soil coefficient of restitution B, soil-steel static friction coefficient F, are significant on the simulation results. The smaller the soil-soil coefficient of restitution, the greater the energy loss during collision of soil particles, which will limit the movement between soil particles and make the static accumulation angle increase. The remaining parameters have p-values greater than 0.05, the effect on the simulation results is extremely small. From Table 5, it can be seen that the soil-steel static friction coefficient F, JKR surface energy H is extremely significant on the dynamic angle of repose with p-value less than 0.01, and p-value of the rest of the parameters is greater than 0.05, the effect on the dynamic angle of repose being extremely small.

Table 4

ANOVA results of the Plackett-Burman test for the static angle of repose

Source	Sum of squares	DF	Mean Square	F-value	P-value	Significance
Model	594.37	8	74.30	20.20	0.0156	*
A	0.3072	1	0.3072	0.0835	0.7914	
B	110.90	1	110.90	30.16	0.0119	*
C	5.07	1	5.07	1.38	0.3251	
D	399.28	1	399.28	108.58	0.0019	**
E	1.67	1	1.67	0.4548	0.5484	
F	46.18	1	46.18	12.56	0.0383	*
G	24.03	1	24.03	6.53	0.0835	
H	6.93	1	6.93	1.88	0.2634	

Table 5

ANOVA results of the Plackett-Burman test for the dynamic angle of repose

Source	Sum of squares	DF	Mean Square	F-value	P-value	Significance
Model	442.08	8	55.26	14.06	0.0262	*
A	30.72	1	30.72	7.82	0.0681	
B	0.4641	1	0.4641	0.1181	0.7538	
C	25.52	1	25.52	6.49	0.0841	
D	19.51	1	19.51	4.96	0.1122	
E	0.9747	1	0.9747	0.2480	0.6527	
F	174.35	1	174.35	44.36	0.0069	**
G	30.53	1	30.53	7.77	0.0686	
H	160.02	1	160.02	40.71	0.0078	**

Note: * indicates a significant difference ($p<0.05$); ** indicates a highly significant difference ($p<0.01$).

Steepest Ascent Test

The steepest ascent test is used to accurately determine the centre point of the test factor levels, enabling the initial response region to quickly approach the optimal response region. Based on the results of the parameter screening tests, the factors with P-values less than 0.05 in Tables 4 and 5 were selected for the steepest ascent test. The selected parameters were gradually increased according to the chosen ascent step size, while the remaining parameters were held constant at intermediate levels: soil shear modulus (1×10^7 Pa), soil-soil static friction coefficient (0.68), soil-steel restitution coefficient (0.45), and soil-steel rolling friction coefficient (0.30). The test results are presented in Table 6. As shown in the table, both the static and dynamic angles of repose increased progressively with higher values of the selected test factors.

Table 6

Steepest Ascent Test Scheme and Results

Serial number	Experimental factors				Static angle of repose / (°)	Dynamic angle of repose / (°)
	B	D	F	H		
1	0.75	0.05	0.5	0.1	25.62	35.61
2	0.63	0.08	0.56	0.14	31.49	47.57
3	0.51	0.11	0.62	0.18	35.6	56.34
4	0.39	0.14	0.68	0.22	38.35	59.95
5	0.27	0.17	0.74	0.26	41.73	62.1
6	0.15	0.2	0.8	0.3	42.05	67.49

Box-Behnken test and regression analysis

In order to obtain the mathematical regression model of the angle of repose with the significant influencing factors (soil-soil restitution coefficient, soil-soil rolling friction coefficient, soil-steel static friction coefficient, and JKR surface energy), a response surface test was conducted using the Box-Behnken method. According to the results of the steepest ascent test, the parameter values of test No. 2 in Table 7 were selected as the intermediate level, and the parameter values of No. 1 and No. 3 were selected as the low level and high level, respectively, for the experimental design. The test scheme and results are shown in Table 7.

Table 7

Box-Behnken test scheme and results

Serial number	Experimental factors				Static angle of repose / (°)	Dynamic angle of repose / (°)
	B	D	F	H		
1	0.51	0.05	0.56	0.14	29.89	48.74
2	0.63	0.05	0.5	0.14	28.94	45.06
3	0.75	0.08	0.56	0.18	30.54	54.77
4	0.63	0.05	0.56	0.18	31.24	53.88
5	0.63	0.08	0.56	0.14	32.92	51.39
6	0.63	0.11	0.5	0.14	34.34	47.28
7	0.75	0.08	0.62	0.14	27.61	53.83
8	0.63	0.11	0.56	0.1	34.93	43.28
9	0.51	0.11	0.56	0.14	35.12	49.71
10	0.75	0.08	0.5	0.14	29.96	44.09
11	0.63	0.05	0.56	0.1	28.52	40.94
12	0.63	0.08	0.56	0.14	32.74	51.94
13	0.63	0.08	0.56	0.14	32.41	51.53
14	0.75	0.08	0.56	0.1	30.51	41.59
15	0.51	0.08	0.56	0.18	33.72	54.53
16	0.63	0.08	0.62	0.1	28.97	46.72
17	0.51	0.08	0.5	0.14	31.43	47.71
18	0.75	0.05	0.56	0.14	27.8	48.9
19	0.63	0.08	0.56	0.14	32.74	51.8
20	0.51	0.08	0.56	0.1	30.79	44.45
21	0.63	0.11	0.62	0.14	31.57	53.67
22	0.63	0.08	0.5	0.1	31.48	36.8
23	0.63	0.08	0.56	0.14	32.66	51.3
24	0.63	0.11	0.56	0.18	34.8	54
25	0.63	0.05	0.62	0.14	28.14	52.58
26	0.63	0.08	0.62	0.18	30.7	55.08
27	0.63	0.08	0.5	0.18	32.23	52.08
28	0.75	0.11	0.56	0.14	32.72	49.83
29	0.51	0.08	0.62	0.14	30.58	52.74

Tables 8 and 9 show the analysis of variance (ANOVA) for the static and dynamic angle of repose in the test, respectively. As can be seen from Tables 8 and 9, the p-values (p-value is the probability of obtaining the observed value of the test statistic and other values that are more unsupportive of the original hypothesis when the original hypothesis is true) of the two fitted models are less than 0.01, indicating that the relationship between the angle of repose and the resulting regression equations is highly significant; the p-values of the out-of-fit terms are all greater than 0.05, indicating that the regression equations are not out-of-fit, and they have a predictive significance; the coefficients of determination for the static angle of repose are 0.9946 for static angle of repose and 0.9926 for dynamic angle of repose, indicating a good fit. For the static angle of repose, the p-values of the soil-soil restitution coefficient B, the soil-soil dynamic friction coefficient D, the soil-steel static friction coefficient F, the JKR surface energy H, and the interaction terms BF, BH, DF, and DH are less than 0.01, which are extremely significant on the static angle of repose; the p-values of each of the quadratic terms, except for H2 and the quadratic term BD are all greater than 0.05, which indicates that these two factors were not significant on the static angle of repose, and all other factors had significant effects on the static angle of repose. For the dynamic angle of repose, the p-values of soil-soil rolling friction factor D, soil-steel rolling friction coefficient F, JKR surface energy, interaction term BF, and secondary terms B2, D2, F2, and H2 are less than 0.01, which are extremely significant on the dynamic angle of repose, and the p-values of soil-soil restitution coefficient B and interaction term BH are less than 0.05, which have a significant effect on the dynamic angle of repose. and the other factors were not significant on the dynamic angle of repose.

Table 8

Analysis of variance of a quadratic regression model for static angle of repose

Source	Sum of squares	DF	Mean Square	F-value	P-value	Significance
Model	127.80	14	9.13	182.58	< 0.0001	**
B- Soil-Soil restitution coefficient	12.79	1	12.79	255.88	0.0290	*
D- Soil-soil rolling friction factor	69.84	1	69.84	1396.96	0.0018	**
F- Soil-steel static friction factor	9.74	1	9.74	194.78	< 0.0001	**
H- JKR surface energy	5.37	1	5.37	107.48	< 0.0001	**

Source	Sum of squares	DF	Mean Square	F-value	P-value	Significance
BD	0.0240	1	0.0240	0.4805	0.9729	
BF	0.5625	1	0.5625	11.25	0.0011	**
BH	2.10	1	2.10	42.05	0.0179	*
DF	0.9702	1	0.9702	19.41	0.3449	
DH	2.03	1	2.03	40.62	0.0754	
FH	0.2401	1	0.2401	4.80	< 0.0001	**
B²	8.12	1	8.12	162.36	0.0040	**
D²	0.2625	1	0.2625	5.25	0.0002	**
F²	18.94	1	18.94	378.79	0.0001	**
H²	0.1434	1	0.1434	2.87	< 0.0001	**
Residual	0.6999	14	0.0500			
Lack of Fit	0.5628	10	0.0563	1.64	0.0501	
Pure Error	0.1371	4	0.0343			
Cor Total	128.50	28				

The quadratic regression equation for the static angle of repose (SAoR) was derived by eliminating the insignificant terms from the model, while ensuring that the remaining terms retained overall model significance and goodness of fit.

$$SRA = 32.69 - 1.03B + 2.41D - 0.9008F + 0.6692H - 0.375BF - 0.725BH + 0.245FH - 1.12B^2 - 0.2012D^2 - 1.71F^2 - 0.1487H^2 \quad (7)$$

Table 9

Analysis of variance for quadratic regression modeling of dynamic angle of repose

Source	Sum of squares	DF	Mean Square	F-value	P-value	significance
Model	630.22	14	45.02	134.73	< 0.0001	**
B- Soil-Soil restitution coefficient	1.98	1	1.98	5.92	0.0290	*
D- Soil-soil rolling friction factor	4.90	1	4.90	14.67	0.0018	**
F- Soil-steel static friction factor	144.21	1	144.21	431.63	< 0.0001	**
H- JKR surface energy	414.89	1	414.89	1241.77	< 0.0001	**
BD	0.0004	1	0.0004	0.0012	0.9729	
BF	5.55	1	5.55	16.60	0.0011	**
BH	2.40	1	2.40	7.19	0.0179	*
DF	0.3192	1	0.3192	0.9554	0.3449	
DH	1.23	1	1.23	3.69	0.0754	
FH	11.97	1	11.97	35.83	< 0.0001	**
B²	3.94	1	3.94	11.78	0.0040	**
D²	8.67	1	8.67	25.96	0.0002	**
F²	9.11	1	9.11	27.27	0.0001	**
H²	36.59	1	36.59	109.52	< 0.0001	**
Residual	4.68	14	0.3341			
Lack of Fit	4.38	10	0.4383	5.96	0.0501	
Pure Error	0.2943	4	0.0736			
Cor Total	634.89	28				

The quadratic regression equation for the dynamic angle of repose (DAoR) was developed by removing the statistically insignificant terms, while ensuring that the model remained significant and exhibited a good fit to the experimental data:

$$DRA = 51.59 - 0.4058B + 0.6392D + 3.47F + 5.88H + 1.18BF + 0.775BH - 0.7789B^2 - 1.16D^2 - 1.19F^2 - 2.38H^2 \quad (8)$$

Determination and validation of discrete element simulation parameters

The experimentally measured soil angles of repose were used as response targets to optimize the regression equations, and the resulting combinations of discrete element simulation parameters were input into EDEM software for validation. Figure 8 presents a comparison between the simulated and experimental values of the optimized parameter sets for each soil layer. The average relative errors for the static angle of repose and dynamic angle of repose were calculated as 1.56% and 0.984%, respectively. These results indicate that the simulated values closely matched the experimental measurements, with no significant differences, thus confirming the accuracy and reliability of the calibrated parameter combinations. Although the angles of repose for each group were relatively similar, different combinations of discrete element simulation parameter values resulted in variations in particle contact interactions and force chain distributions.

These differences led to distinct stacking morphologies in the simulated particle assemblies. Therefore, among the five DEM parameter combinations tested for each soil layer, the one that produced a stacking morphology most closely resembling the actual experimental observation was selected as the preferred combination. The selected optimal DEM parameter values for each soil layer are as follows: soil-soil restitution coefficient (B) is 0.734, 0.556, 0.643, soil-soil rolling friction coefficient (D) is 0.082, 0.086, 0.095, soil-steel static friction coefficient (F) is 0.564, 0.511, 0.525 and the JKR surface energy (H) is 0.102, 0.117, 0.122.

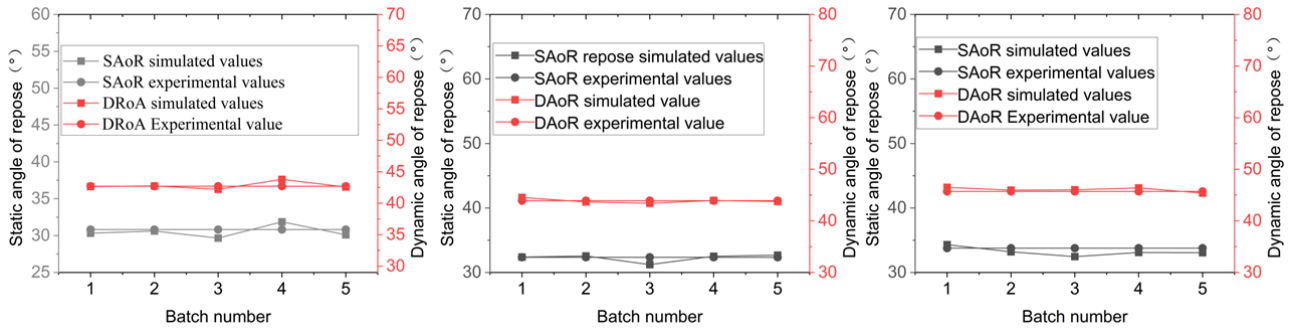

(a) (b) (c)

Fig. 8 - Comparison between simulated and experimental values using the optimized discrete element simulation parameter combinations

The static and dynamic angles of repose for the upper soil layer are shown in Figures 9 and 10. As illustrated, there is no significant difference between the simulation results and the actual experimental observation. The measured static angle of repose was 30.82°, and the dynamic angle of repose was 42.70°, while the simulated values were 30.62° and 42.75°, respectively. The relative errors for the static and dynamic angles of repose were 0.65% and 0.12%, which are both very low. These results confirm that the optimized discrete element simulation parameter combination is accurate and reliable, and thus suitable for use in subsequent simulation studies.

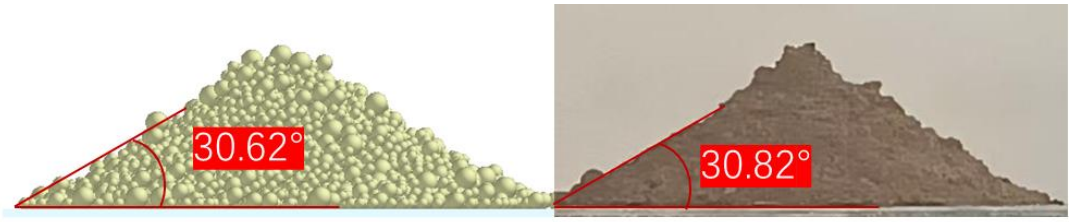

(a) simulated image (b) actual image

Fig. 9 - Static angle of repose of the soil

(a) simulated image (b) actual image

Fig. 10 - Dynamic angle of repose of the soil

CONCLUSIONS

The computational efficiency of discrete element simulations was significantly improved by scaling particle size and reducing particle stiffness. The results of the Plackett-Burman test indicated that, within a certain value range, factors such as particle shear modulus, particle-steel restitution coefficient, particle-steel kinetic friction coefficient, and particle-particle static friction coefficient did not significantly affect the angle of repose. In the Box-Behnken response surface test, the static and dynamic angles of repose were used as dual response indices to optimize the discrete element simulation parameters. This approach led to more accurate simulation results, with particle behaviour more closely resembling actual soil conditions. In this study, the static and dynamic angles of repose were adopted as macroscopic response indicators for calibrating the discrete element simulation parameters of simplified soil particles. Optimal parameter combinations were determined through the Plackett-Burman and Box-Behnken tests, and subsequently validated through experimental comparison. The main conclusions are as follows:

(1) The average static and dynamic angles of repose of the soil were measured using a custom-built device, yielding values of 30.82°, 32.35°, and 33.77° for the static angle, and 42.7°, 43.91°, and 45.7° for the dynamic angle, corresponding to the upper, middle, and lower soil layers, respectively.

(2) The Plackett-Burman test identified that the soil-soil restitution coefficient, soil-soil rolling friction coefficient, and soil-steel static friction coefficient significantly influenced the static angle of repose, while the soil-steel static friction coefficient and JKR surface energy were significant factors for the dynamic angle of repose.

(3) The Box-Behnken test was employed to establish second-order regression models for both static and dynamic angles of repose. These models were optimized using the experimentally measured angle values as targets. The resulting optimal parameter combinations, validated through experiment, were as follows: soil-soil restitution coefficients were 0.734, 0.556, 0.643, soil-soil rolling friction coefficients were 0.082, 0.086, 0.096, soil-steel static friction coefficients were 0.564, 0.511, 0.525, JKR surface energies were 0.102, 0.117, 0.122.

(4) The simulated static angles of repose for the three soil layers were 30.62°, 32.51°, and 33.2°, and the simulated dynamic angles were 42.75°, 43.95°, and 45.96°, respectively. The corresponding relative errors for the static angle were 0.65%, 0.09%, and 2.03%, and for the dynamic angle were 0.28%, 0.12%, and 0.56%. These small errors confirm that the calibrated discrete element simulation parameters are accurate and reliable, and can be confidently used in subsequent DEM simulations.

REFERENCES

[1] Chen Y., Qi Y., Wang Y. (2017). Spatial Variability and Factors Affecting Soil Available Potassium in the Central Qinling – Daba Mountain Area (秦巴中部山区耕地土壤速效钾空间变异及其影响因素) [J]. *Research of Environmental Sciences*, Vol. 30(2), pp.257-266.

[2] Feng Y.T., Han K., Owen D.R.J., Loughran J. (2009) On upscaling of discrete element models: Similarity principles [J]. *Engineering Computations*, Vol. 26(6), pp.599-609.

[3] Han S., Qi J., Li Y. (2021). Parameters Calibration of Discrete Element for Deep Application of Bulk Manure in Xinjiang Orchard (新疆果园深施散体厩肥离散元参数标定研究) [J]. *Transactions of the Chinese Society for Agricultural Machinery*, Vol. 52(4), pp.101-108.

[4] Li S., Liu Y, Li Y., Hu M. (2024). DEM parameters of slope cultivated purple soil in Southwest China and interaction mechanism between very narrow tine [J]. *Scientific Reports*, Vol. 14(1), pp.18089.

[5] Li J., Tong J., Hu B., Ma Y. (2019). Calibration of parameters of interaction between clayey black soil with different moisture content and soil-engaging component in northeast China (不同含水率黏重黑土与触土部件互作的离散元仿真参数标定) [J]. *Transactions of the Chinese Society of Agricultural Engineering*, Vol. 35(6), pp.130-140.

[6] Luana C., Rodrigo C, Maria D. (2017). Flow properties of coarse and fine sugar powders [J]. *Journal of Food Process Engineering*, Vol. 14(1), pp.1-10.

[7] Li Y., Li F., Xu X. (2019). Parameter calibration of wheat flour for discrete element method simulation based on particle scaling (基于颗粒缩放的小麦粉离散元参数标定) [J]. *Transactions of the Chinese Society of Agricultural Engineering*, Vol. 35(16), pp.320-327.

[8] Luo S., Yuan Q., Gouda S. (2018). Parameters Calibration of Vermicomposting Nursery Substrate with Discrete Element Method Based on JKR Contact Model (基于 JKR 粘结模型的蚯蚓粪基质离散元法参数标定) [J]. *Transactions of the Chinese Society for Agricultural Machinery*, Vol. 49(4), pp.343-350.

[9] Lommen S., Schott D., Lodewijks G. (2014). DEM speedup: Stiffness effects on behavior of bulk material [J]. *Particuology*, Vol. 12(4), pp.107-112.

[10] Maitadudulili A., Litipu Y., Abudureheman K. (2016). Technical Key Points of Grape Trenching and Vine Burying Machine Operation (葡萄开沟埋藤机作业技术要点) [J]. *Agricultural Machinery Technology Extension*, Vol. 16(10), pp.52-53.

[11] Song Z., Li H., Tian F., Li F. (2022). Calibration Method of Contact Characteristic Parameters of Soil in Mulberry Field Based on Unequal-diameter Particles DEM Theory (桑园土壤非等径颗粒离散元仿真模型参数标定与试验) [J]. *Transactions of the Chinese Society for Agricultural Machinery*, Vol. 53(6), pp.21-32.

[12] Shen X., Zhu Z., Yang L., Liu J. (2024). Current situation and development suggestions of wine grape mechanization in Xinjiang (新疆酿酒葡萄生产机械化现状与发展趋势) [J]. *Xinjiang Agricultural Sciences*, Vol.61(SI), pp.147-152.

[13] Smith W., Peng H. (2024). Modeling of wheel-soil interaction over rough terrain using the discrete element method [J]. *Journal of Terramechanics*, Vol. 51(5-6), pp.277-287.

[14] Thomas R., André K. (2018). Scaling of the angle of repose test and its influence on the calibration of DEM parameters using upscaled particles [J]. *Powder Technology*, Vol. 330(2018), pp.58-66.

[15] Wang M., Han S., Liu X. (2024). The current development status of the grape industry in Xinjiang (新疆葡萄产业发展现状分析) [J]. *Xinjiang Agricultural Sciences*, Vol. 61(SI), pp.127-130.

[16] Yang Q., He M., Shi L., Li Z. (2023). Calibration of discrete element simulation parameters for interactions between layered cold soil and contact soil cleaning tools (分层防寒土与接触式清土机具相互作用的离散元仿真参数标定) [J]. *Journal of Jiangsu University*, Vol. 44(1), pp.52-61.

[17] Zhang X., Guo R, Shi Z. (2017). Establishment And Calibration of Discrete Element Model for Coated Wheat Seed Based on Static An [J]. *INMATEH -Agricultural Engineering*, Vol. 74(3), pp.370-379. DOI: https://doi.org/10.35633/inmateh-74-32

[18] Zeng Z., Ma X., Cao X (2021). Critical Review of Applications of Discrete Element Method in Agricultural Engineering (离散元法在农业工程研究中的应用现状和展望) [J]. *Transactions of the Chinese Society for Agricultural Machinery*, Vol. 52(4), pp.1-20.

[19] Zhen W., Liu H., Qian X. (2024). Discrete Element Parameter Calibration for Red Soil with Different Moisture Contents in Fujian Tobacco-growing Areas (福建烟区不同含水率红壤离散元参数标定) [J]. *Journal of Shenyang Agricultural University*, Vol. 55(3), pp.323-333.

[20] Zhou P., He M., Kan Z. (2018). Experiment on the Dynamic Angle of Repose of Soil Particles Based on OpenCV-Python (基于 OpenCV-Python 的土壤颗粒动态休止角试验) [J]. *Journal of Chinese Agricultural Mechanization,* Vol. 44(5), pp.214-222.